Polymer Blends in a Contraction−Expansion Flow

Nigel Clarke,*,† Edoardo De Luca,† Julian Bent,† Gavin Buxton,† Tim Gough,‡ Isabelle Grillo,§ and Lian R. Hutchings†

Department of Chemistry, Durham University, Durham DH1 3LE, U.K., School of Engineering, University of Bradford, Bradford BD7 1DP, U.K., and Institut Laue Langevin, 6 rue Jules Horowitz, BP 156 38042 Grenoble Cedex 9, France

Received May 16, 2006; Revised Manuscript Received August 23, 2006

ABSTRACT: We have probed the coupling between flow and concentration fluctuations in polymer blends using small-angle neutron scattering. We utilized a recirculating cell with a slot die, enabling us to measure the behavior at the entrance, within and at the exit of a contraction−expansion flow. While, as expected, anisotropy was observed in all nonquiescent experiments, the correlation lengths associated with the concentration fluctuations are found to be "stretched" more in the direction perpendicular to the flow at all positions along the centerline of the flow, except at the slot die exit. To gain insight into the observations, we present calculations of the scattering based on a multiscale approach, which bridges the gap between macroscopic Newtonian fluid dynamics and the convection of nanoscale concentration fluctuations. However, we find that this model contains insufficient physics to correctly describe our observations. Consequently, we argue that the deformation of the correlation length is primarily due to the coupling between weakly non-Newtonian stresses and thermodynamics.

1. Introduction

It has long been appreciated that flow and structure are coupled in polymer solutions and mixtures. Since polymers are often subjected to flow during processing, it is desirable to be able to explain and predict the effect of flow on the microstructure and, as a consequence, on the properties of the final material. The impact of a flow field on microstructure ranges from shear-induced crystallization in polymer melts to shear-induced mixing in polymer blends. It is the latter which is the subject of this paper.

Studies of polymer blends in simple shear flows have found shifts, some of which are significant, of the apparent phase-separation temperature. One of the earliest studies on polymer blends was reported by Mazich and Carr,[1] who observed a slight increase in the temperature at which phase separation occurred during heating of a polystyrene/polyvinylmethyl ether blend when it was subject to a shear flow. In a more wide ranging series of experiments,[2] involving blends exhibiting lower critical solution temperature behavior, it has been found that shear-induced demixing and shear-induced mixing may be observed within the same blend depending on the magnitude of the applied flow. A brief overview of other experimental studies[3−10] of blends subjected to shear flows can be found in a recent review article.[11]

The range of observed behaviors is a direct consequence of the complexity of the rheological behavior of mixtures, even when they are not phase separated. A number of different models have been proposed to explain such behavior.[11] For example, the observations outlined in the previous paragraph have been explained, at least qualitatively, by theories that modify the equilibrium thermodynamics with an elastic energy term[12] and by theories that use equations of motion for concentration fluctuations as their starting point.[13] The main feature both approaches have in common is that concentration dependent normal stresses are required for there to be shifts in the phase boundary or, more precisely, shifts in the limits of stability.

The phase-separation dynamics of a polystyrene/polyvinyl methyl ether blend under shear flow have also been examined with light scattering.[14] It was found that the phase-separation behavior at the early stage could be described qualitatively by Cahn−Hilliard[15] linearized theory, modified to account for the effects of flow-induced stress.

While shifts in the phase boundaries are of interest, we believe that a more sensitive probe of the effect of flow can be provided by studying concentration fluctuations. In the quiescent state, these fluctuations give rise to distinct scattering patterns, the magnitude of which increases as a phase boundary is approached. Such patterns are measurable by small-angle neutron scattering (SANS) if one component is deuterated. This fact has resulted in SANS being an established technique for determining interaction parameters in the quiescent state. The random phase approximation (RPA),[16] predicts that at equilibrium, the wavevector, **q**, dependent structure factor is given by

$$S(\mathbf{q}) = \frac{1}{2(\chi_S - \chi + \kappa q^2)} \tag{1}$$

where χ is the enthalpic interaction parameter, κ is the interfacial tension and χ_S is the value of the interaction parameter on the quiescent spinodal. The latter two parameters depend on the volume fractions, ϕ_A and ϕ_B, of the two components in the mixture. According to the Flory−Huggins theory for polymer blends,[17] if incompressibility, i.e., $\phi_B = 1 - \phi_A$, is assumed

$$\chi_s = \frac{1}{2}\left(\frac{1}{N_A\phi_A} + \frac{1}{N_B\phi_B}\right) \tag{2}$$

where N_A and N_B are the degrees of polymerization of each component, and deGennes[16] has shown that $\kappa = b^2/36\phi_A(1 - \phi_A)$.

Clearly, it is to be expected that concentration fluctuations will be affected by flow. To date, we are only aware of one study in which concentration fluctuations of polymer blends

* Corresponding author. E-mail: nigel.clarke@durham.ac.uk.
† Department of Chemistry, Durham University
‡ School of Engineering, University of Bradford.
§ Institut Laue Langevin.

10.1021/ma0610966 CCC: $33.50
Published on Web 10/03/2006

subjected to a shear flow have been probed by neutron scattering.[18] Two different blends, one exhibiting lower critical solution temperature behavior and the other exhibiting upper critical solution temperature, were studied using a concentric cylinder shear cell. For both blends it was found that fluctuations were suppressed by the shear flow.

The advantage of studying concentration fluctuations is that the consequences of flow may be expected to be closely related to the blend rheology. While the one-phase region remains stable, it is possible to unambiguously determine the blend viscosity and, therefore, interpret results within a framework that includes a known rheological response. Once a blend becomes unstable, the blend rheology becomes dependent on the microstructures that develop, which may or may not reach a steady-state. Hence, scattering under flow within the one-phase region provides a unique opportunity for quantitative comparisons with theory, as has been highlighted recently by experiments[19,20] and theory[21,22] for the enhancement of concentration fluctuations in a concentrated polymer solution subjected to an oscillatory flow.

Although shear is attractive to explore due to the relative simplicity with which steady state and oscillatory conditions can be established, industrial flows are often more complex. As noted by Rothstein and McKinley,[23] the contraction−expansion flow has been long regarded as a standard for the study of complex flows that contain elements of strong shear, uniaxial extension and biaxial expansion. The main aim of the present work is the investigation of a blend in such a flow by small-angle neutron scattering.

In addition, we develop a multiscale approach that enables the structure factor for the polymer blend to be calculated from a flow simulated using the lattice Boltzmann (LB) technique. From this we are able to gain additional insight into the role that fluid dynamics plays in determining the magnitude and orientation of the concentration fluctuations. On the basis of the outcome of these simulations, we then speculate on the additional physics required to explain our observations, and suggest a simple way in which the experiments can be interpreted.

2. Experimental Section

Materials. Deuterated poly(styrene-d_8) (M_w = 60 300 g mol^{-1}, PDI = 1.04) was synthesized by anionic polymerization using standard high vacuum techniques. Benzene was used as the solvent and *s*-butyllithium as the initiator. Poly(α-methylstyrene) (M_w = 57 800 g mol^{-1}, PDI = 1.1) was similarly prepared using anionic polymerization using the same initiator and THF as the solvent. The polymerization was carried out at −70 °C according to the procedure of Kim and Han.[24]

To obtain a 70/30 w/w blend of these two polymers, and to ensure blending at a molecular level the two polymers were dissolved in a common solvent (5% w/v in THF) and stirred in solution for an hour. The polymer blend was recovered by precipitation, by adding the polymer solution to approximately 10 times the volume of a common nonsolvent (methanol). The resulting precipitate was collected by filtration and dried to constant mass in vacuo. This blend exhibits UCST behavior;[25] i.e., it phase separates upon cooling.

Flow Cell. The contraction−expansion flow was achieved by the use of a recirculating extruder with a slot die contraction 8:1. The exact geometry of the cell, including the positions at which measurements were taken, is shown in Figure 1. In Table 1, we define the position of the beam with respect to the entrance of the contraction, the position numbers indicated will be referred to throughout the remainder of the paper. For a blend with similar molecular weights in which the polystyrene and poly(α-methylstyrene) had molecular weights, M_w = 49 000 g mol^{-1} and M_w = 56 400 g mol^{-1}, respectively, the spinodal temperature, for a blend with 30% poly(α-methylstyrene), has been measured as[25] ∼450 K. From their values of the interaction parameter, determined from fitting observed cloud points for a range of compositions to the Flory−Huggins theory, we estimate that the spinodal temperature of the blend utilized in this paper is ∼457 K, well below 493 K, the temperature at which the experiments reported herein were performed.

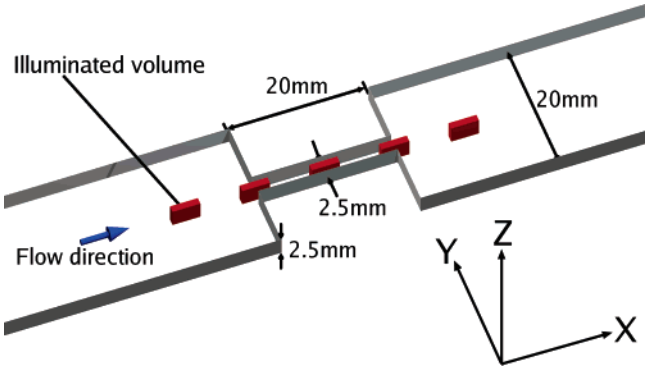

Figure 1. Illustration of the flow cell geometry. The channel width is contracted from 20 mm to 2.5 mm for a distance of 20 mm in the center of the cell. The thickness of the cell is 2.5 mm. Also shown are the five beam positions, referred to as 1 through 5 in the text.

Table 1. Defining the Geometry of the Cell, with the Position of the Center of the Beam in the *x* Direction with Respect to the Entrance of the Contraction along the Center Line of the Cell

position number	center of beam (mm)
1	−10
2	0
3	10
4	20
5	30

The flow field through the cell is dependent on the volumetric flow rate, which in the current study has a maximum value of 0.3 cm^3 s^{-1}. Flow rates are controlled by an electric motor connected to a gear pump; full details can be found elsewhere.[26,27]

Small-Angle Neutron Scattering. SANS was performed using the D22 diffractometer at the Institut Laue Langevin in Grenoble (France). The sample−detector distance used was 4 m with an incident beam aperture of 4 × 1 mm and an incident wavelength of 10 Å. For each sample, both transmission and scattering spectra were obtained. In addition, to determine detector efficiency, calculation of the absolute scattering and the subtraction of background scattering, transmission for the empty holder, and transmission and scattering from the empty cell and from a water sample were all measured. From the reduced two-dimensional scattering spectra, vertical and horizontal sector averaged distribution curves were obtained.

Rheology. Frequency sweep and viscosity measurements on the blend were performed using a TA AR2000 rheometer with a plate−plate geometry (radius of 25 mm and gap 0.9 mm) at a temperature of 493 K.

3. Results and Discussion

The viscosity of the blend was found to be 128 Pa·s. As can be seen in Figure 2, from the frequency sweep rheology, it was not possible to directly determine the longest relaxation time, τ_L, since at 493 K, no crossover between the loss modulus and storage modulus was observed. Extrapolation to higher frequencies suggests that $\tau_L \sim 10^{-3}$ s.

A comparison of GPC traces of the blend before and after the experiments show the appearance of a slight tail, which can be attributed to polymer degradation. Subsequent analysis suggests a ∼4% degradation of the polymer.[28]

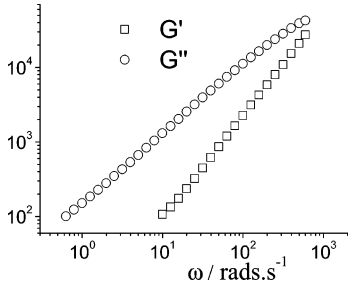

Figure 2. Frequency dependence of the storage, G', and the loss, G'', modulus, for the blend at 493 K.

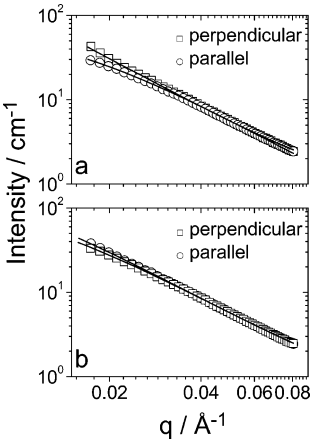

Figure 3. Scattering profiles for parallel and perpendicular to the flow at the maximum flow rate at (a) position 2 and (b) position 5. The solid lines show the fit to eq 3.

Typical examples of the sector averaged (over 45°) absolute scattering can be seen in Figure 3, for positions 2 and 5, which show clear anisotropy between the scattered intensity in the flow direction (parallel) and the direction perpendicular to the flow. Such anisotropy was observed in all nonquiescent experiments.

Rather surprisingly we found that the sector averaged data were still well described by a simple Ornstein−Zernike form

$$S(q) = \frac{S_0}{(1 + q^2\xi^2)} \tag{3}$$

where ξ is a correlation length, which varies with flow rate, direction with respect to the flow and the position of the beam with respect to the slot die. For quiescent blends the extrapolated value, S_0, of the scattering at $q = 0$ can be directly related to the interaction parameter of the blend, by the relation

$$S_0 = \frac{V\nu_0(\rho_b^{dPS} - \rho_b^{P\alpha MS})^2}{2(\chi_S - \chi)} \tag{4}$$

where V is the illuminated scattering volume, ν_0 is a reference volume (taken as 176×10^{-22} cm^3), and $\rho_b^{dPS} = 6.42 \times 10^{10}$ cm^{-2} and $\rho_b^{P\alpha MS} = 1.23 \times 10^{10}$ cm^{-2} are the neutron scattering length densities for deuterated polystyrene and poly(α-methylstyrene), respectively. For the quiescent blend, we find $\chi = 9.5 \times 10^{-4}$at $T = 493$ K. We are not aware of any other direct measurements of the interaction parameter for this blend. Lin and Roe[25] determined the interaction parameter by fitting the Flory−Huggins expression, eq 2, to the measured phase boundary for a range of compositions. Extrapolation of their results leads to the prediction that $\chi \sim 3 \times 10^{-3}$ at $T = 493$ K, a factor of 3 greater than our measured value. This discrepancy is presumably a consequence of the indirect method utilized in ref 25, and the difference in temperatures (between 450 and 470 K in ref 25, and 493 K in this paper) at which the interaction parameter was deduced.

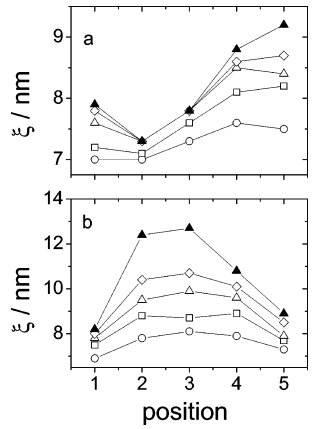

Figure 4. Correlation length for the different positions and flow rates: ○ = 0.06 cm^3 s^{-1}, □ = 0.10 cm^3 s^{-1}, △ = 0.16 cm^3 s^{-1}, ◇ = 0.22 cm^3 s^{-1}, ▲ = 0.30 cm^3 s^{-1}, for (a) the direction parallel to the flow and (b) the direction perpendicular to the flow. From the fitting of the scattering to eq 3, errors in the correlation length are typically ∼3%; however, for clarity, error bars are not shown.

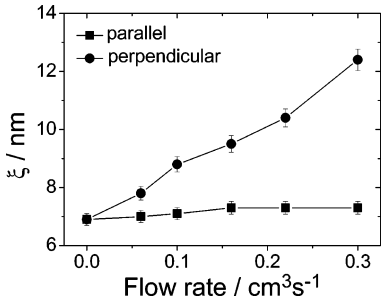

Figure 5. Correlation lengths parallel and perpendicular to the flow at position 2 as a function of flow rate.

As can be seen from Figure 4, the correlation length is greater in the direction perpendicular to the flow for positions 1−4. On the other hand, at position 5, after the exit from the slot die, the correlation length is greater in the direction parallel to the flow. These trends are counter to what would be qualitatively anticipated from consideration of convection effects alone, as will be quantitatively verified in the following section. The greatest difference between the correlation lengths in the parallel and perpendicular directions was found for position 2. That the greatest "deformation" of the fluctuations should occur at this position is expected, since this is the region within the cell at which the velocity gradients associated with the flow field are at their most significant, again as will be highlighted in the following section. At position 5, on the other hand, the correlation length is greater in the direction of the flow than in the perpendicular to the flow direction, so that at the exit of the die the concentration fluctuations are enhanced in the flow direction. Furthermore, as illustrated in Figure 5 for position 2, there is a stronger dependence of the correlation length on the flow rate in the perpendicular direction than in the parallel direction. Indeed, in particular for positions 2 and 3, the correlation length in the parallel direction appears to reach a plateau value when the flow rate reaches 0.1 cm^3 s^{-1}. It is worth noting that at this flow rate, the maximum extension and shear rates experienced by the blend are $\dot{\epsilon} \sim 30$ s^{-1} and $\dot{\gamma} \sim 60$ s^{-1}, respectively (see next section). Hence the dimensionless (Weissenberg) numbers characterizing the flow ($\dot{\epsilon}t_L$ and $\dot{\gamma}t_L$) are both much less than unity, suggesting that nonlinear flow

effects (e.g., shear-thinning) are unimportant. We also note that, for any given flow rate, the correlation length perpendicular to the flow is a maximum at position 3, whereas in the direction parallel to the flow the correlation length is a minimum at position 2.

Because of the fact that the deformation is observed to be more significant in the direction perpendicular to the flow at all positions except position 5, we believe that the increase in correlation length is due purely to the coupling between stress and thermodynamics, rather than stress and chain dimensions. If the effects were due to chain stretching, the exact opposite trend would be observed.

In the following sections, we attempt to develop a framework within which we can understand these results. First, we address to what extent simple convection can account for our results. While it may be anticipated from the above discussion that such effects are not sufficient, it is nonetheless instructive to consider this question quantitatively in view of the complexity of the flow field. In particular, the scattering is averaged over a volume within which there is pure extension along the centerline and mixed shear and extension away from the centerline.

Background Theory. We briefly review some of the relevant developments with regards to theories for predicting the response of polymer blends to flow. We note that no work has yet been undertaken that is directly applicable to the experiments described in this paper. Most theoretical treatments have focused on simple shear flow, and analytical predictions for scattering are restricted to the flow gradient and vorticity directions, for reasons that will be outlined in a later section. The dynamics of a polymer blend can be captured using the Cahn−Hilliard−Cook[15,29] model, which describes how diffusion couples with thermodynamics in a binary system. For an incompressible blend in which the local volume fraction of component A is $\phi_A(\mathbf{r},t)$, the structure factor, defined by $S(\mathbf{q},t) = \langle|\delta\phi_A(\mathbf{q},t)|^2\rangle$, where $\delta\phi_A(\mathbf{q},t) = \int\delta\phi_A(\mathbf{r},t)\exp\{-i\mathbf{q}\cdot\mathbf{r}\}\,d\mathbf{r}$, evolves according to

$$\frac{\partial S(\mathbf{q},t)}{\partial t} = -4q^2M[(\chi_S - \chi) + \kappa q^2]S(\mathbf{q},t) + 2Mq^2 \quad (5)$$

where M is the kinetic coefficient, or mobility. The first term on the right-hand side of eq 5 represents the diffusion of concentration fluctuations, with a rate that depends on both the underlying kinetics and the thermodynamic driving force (i.e., closer to the phase boundary, fluctuations become longer lived). The second term on the right-hand side represents the effect of noise. At equilibrium, i.e., $\partial S(\mathbf{q},t)/\partial t = 0$, eq 5 reduces to the correct form of the structure factor given by eq 1.

The simplest extension of the Cahn−Hilliard−Cook model to include shear is to assume that the only consequence is that concentration fluctuations are convected with the macroscopic flow field, as suggested by Lai and Fuller,[30] adopting a model proposed by Ohta et al.[31] With such an assumption, stress, and hence flow rate, gradients are neglected. This is only likely to be a physically realistic assumption if the viscoelastic properties of the two components are identical. In a shear flow, characterized by a shear rate, $\dot\gamma$, the equation of motion is then a simple modification of eq 5

$$\frac{\partial S(q,t)}{\partial t} - \dot\gamma q_x\frac{\partial S(\mathbf{q},t)}{\partial q_y} = -4q^2M[(\chi_S - \chi) + \kappa q^2]S(\mathbf{q},t) + 2Mq^2 \quad (6)$$

where q_x, q_y, and q_z are the wavevectors in the flow, the flow-gradient and the vorticity directions respectively, and $q^2 = q_x^2 + q_y^2 + q_z^2$. The second term on the left-hand side of eq 6 represents the convective effect of shear. The steady-state solution to eq 6, is

$$\left[4Mq^2(\chi_S - \chi + \kappa q^2) - \dot\gamma q_x\frac{\partial}{\partial q_y}\right]S(\mathbf{q},t) = 2Mq^2 \quad (7)$$

However, this is still a differential equation in the variable q_y, and a simple analytical interpretation is not straightforward. Hence, even for a minimal extension to the Cahn−Hilliard−Cook theory for a simple shear flow, we see that a quantitative interpretation of experimental results requires numerical input from theory.

Flow Field in a Contraction Cell for a Newtonian Fluid. To gain insight into the complex flow field within a contraction−expansion cell, we use the LB technique to capture the 3-dimensional hydrodynamics of the fluid flow through the slot die. For brevity, we refer the interested reader to the review paper by Chen and Doolean[32] for an overview, and other references[33−35] for a more in depth description, of the multirelaxation LB model used in the current work.

We simulate the behavior of a Newtonian fluid with a viscosity that matches that of the blend. Furthermore, we assume that the concentration fluctuations in the miscible polymer blend are sufficiently small that the system can be described with a single fluid phase. While we recognize that this does not capture all of the physics associated with the flow of an entangled polymeric liquid, it nonetheless serves as a useful starting point. The LB technique is an efficient method for simulating the hydrodynamics of a Newtonian fluid.[32] Specifically, it enables systems with complex geometries to be modeled with relative ease.[36] This technique differs from conventional numerical schemes, which involve the direct discretization of the continuum equations, in that the LB model incorporates the "microscopic" physics of fluid behavior. In particular, the LB method consists of "particles" of fluid propagating and colliding on a simple lattice such that the averaged, long-wavelength properties of the system obey the desired Navier−Stokes equation.[37]

To map the fluid flow in the actual experiments to the simulated fluid flow, we compare the Reynolds numbers for the two systems. From the maximum volumetric flow rate, the maximum of the spatially averaged velocity along the centerline of the cell is $\bar v = 0.048$ m s^{-1}. Given the density of the fluid is $\rho \sim 1 \times 10^3$ kg m^{-3} and the viscosity is $\eta = 128$ Pa·s the Reynolds number is given by, $Re = \rho\bar v 2.5\text{ mm}/\eta \approx 9.4 \times 10^{-4}$.

In the simulation we assume that the dimensionless density is unity and that the hydrodynamic stresses relax instantaneously to equilibrium resulting in a dimensionless viscosity of $\eta = {}^1/_6$. The lattice spacing in real units is taken to be 0.1 mm (the cross-sectional dimension of the central channel is, therefore, $25\Delta x$ by $25\Delta x$) which results in a Reynolds number of $Re = 150\ \bar v$. By varying the value of velocity in the system we can match the Reynolds numbers for the experimental and simulated systems and, therefore, capture the contractile fluid flow through the slot die. Figure 6 shows the flow profile through the cell. The fluid velocity is represented, both in magnitude and orientation, by the red cones. The gray walls represent the boundaries of the flow cell. The cones are positioned along streamlines which represent the path of fluid elements through the simulation. For clarity, we present only flow profiles in the central plane, corresponding to $z = 0$, but we emphasize that our simulations are 3-dimensional. The cones are positioned along these streamlines at regular equitime intervals. That is, the distance between sequential cones along a sreamline

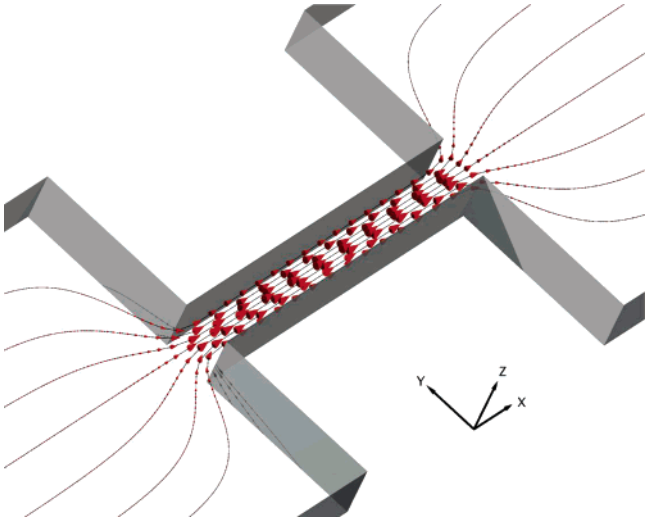

Figure 6. Flow profile through the cell. The fluid velocity is represented, both in magnitude and orientation, by the red cones. The gray walls represent the boundaries of the flow cell. The cones are positioned along sreamlines at regular equi-time intervals.

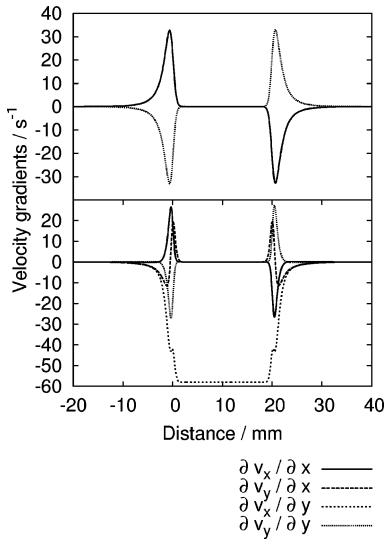

Figure 7. Gradients of the flow field along the center (upper) and off-center (lower) streamlines as a function of distance through the cell. The inlet of the slot die is at 0 mm and the exit is at 20 mm.

represent the distance moved by the fluid element in 2×10^{-2} s.

The velocity at the walls is zero (no-slip boundary conditions) and reaches a maximum in the center of the channel. The velocity of the fluid is relatively small outside of the slot die and increases dramatically as the fluid channel is contracted. Fluid from all sections of the outer channel come together at the entrance of the slot die and this results in an increase in fluid velocities. As the fluid emerges from the end of the slot die, it must fill the larger volume, and hence, the magnitude of the velocities is significantly reduced.

To gain insight into the effects of this macroscopic flow profile on the microscopic polymer blend concentration fluctuations it is necessary to consider the spatial gradients of the fluid velocity as this characterizes the amount of shear and stretching to which the fluid is subjected. We, therefore, follow mesoscopic fluid elements as they travel through the system and monitor the spatial gradients of velocity as a function of time. Figure 7 shows the magnitude of these gradients as a function of the distance the fluid has travelled in the x direction. The upper graph in Figure 7 shows the velocity gradients for a fluid element travelling through the center of the system. The magnitude of the velocity in the x-direction increases abruptly at the inlet of the slot die and decreases at the exit, as indicated by the increase and decrease in $\partial v_x/\partial x$. This increase and decrease in fluid velocity in the x-direction is fuelled by the contraction of the fluid and, hence, velocity components in the y-direction. This can be seen as the decrease in $\partial v_y/\partial y$ at the inlet as fluid just outside the slot die is flowing down toward the slot die from the top of the cell and up from the bottom of the cell.

The lower graph in Figure 7 shows the velocity gradient for a fluid element which is travelling off center. That is, the fluid element originally starts 5 mm from the central streamline in the y-direction, and moves in toward the central streamline as the fluid travels through the slot die (coming to a distance of 0.5 mm from the centerline), before returning to a straight trajectory 5 mm from the center after it emerges from the slot die. The velocity gradients $\partial v_x/\partial x$ and $\partial v_y/\partial y$ are similar to the case shown in the upper figure of Figure 7, however now the velocity gradients $\partial v_x/\partial y$ and $\partial v_y/\partial x$ are no longer negligible. The velocity gradient $\partial v_y/\partial x$ decreases before the inlet and increases just afterward because of the local increase in velocity in the y-direction as fluid flows into the inlet of the slot die. The final velocity gradient of consequence is $\partial v_x/\partial y$ and represents the shearing of the fluid along this sreamline. The fluid velocity is a maximum in the center of the channel and is zero at the no-slip boundaries. There are, therefore, velocity gradients in the y-direction which are significantly higher in the slot die where the magnitude of the velocity field is greater and the channel width is narrower. This, in effect, causes a dramatic increase in the magnitude of $\partial v_x/\partial y$ in the slot die. This also allows us to estimate the Weissenberg number, defined as the product of the relaxation time (10^{-3} s) and the deformation rate (which from Figure 6 can be seen to be $\sim$60 s^{-1}). The Weissenberg number is, therefore, $\sim$0.06 which is small enough that non-Newtonian effects on the flow profile can be considered negligible.

Convective Effects on the Structure Factor. We now present an extension to the LB simulations, in which we employ a multiscale approach where the local velocity gradients are taken into consideration when evolving the structure factor for the polymer blend concentration fluctuations. In this manner, we can determine the microscopic structure factor for an element of fluid, as it traverses the macroscopic slot die, experiencing variations in the local velocity field.

At all points within the flow cell, the velocity takes the form

$$\mathbf{v} = \begin{pmatrix} v_{x0} + \dfrac{\partial v_x}{\partial x}x + \dfrac{\partial v_x}{\partial y}y + \dfrac{\partial v_x}{\partial z}z \\ v_{y0} + \dfrac{\partial v_y}{\partial x}x + \dfrac{\partial v_y}{\partial y}y + \dfrac{\partial v_y}{\partial z}z \\ v_{z0} + \dfrac{\partial v_z}{\partial x}x + \dfrac{\partial v_z}{\partial y}y + \dfrac{\partial v_z}{\partial z}z \end{pmatrix} \tag{8}$$

where v_{x0}, v_{y0}, and v_{z0} are the background velocity fields, which are not important to the local variations in composition (note that only gradients in the velocity field will result in the stretching or rotating of polymer fluctuations). The remaining terms in the above expression for the velocity take into consideration the local gradients in the velocity field.

Using the generalized velocity field given by eq 8, and assuming that the fluctuations are small we can write the evolution of the structure factor in the following form:

$$\frac{\partial S(\mathbf{q},t)}{\partial t} + \left\{ q_x \left[\frac{\partial v_x}{\partial x}\frac{\partial}{\partial q_x} + \frac{\partial v_x}{\partial y}\frac{\partial}{\partial q_y} + \frac{\partial v_x}{\partial z}\frac{\partial}{\partial q_z} \right] + q_y \left[\frac{\partial v_y}{\partial x}\frac{\partial}{\partial q_x} + \frac{\partial v_y}{\partial y}\frac{\partial}{\partial q_y} + \frac{\partial v_y}{\partial z}\frac{\partial}{\partial q_z} \right] + q_z \left[\frac{\partial v_z}{\partial x}\frac{\partial}{\partial q_x} + \frac{\partial v_z}{\partial y}\frac{\partial}{\partial q_y} + \frac{\partial v_z}{\partial z}\frac{\partial}{\partial q_z} \right] \right\} S(\mathbf{q},t) = -4Mq^2[\chi_s - \chi + \kappa q^2]S(\mathbf{q},t) + 2Mq^2 \quad (9)$$

The time evolution of $S(\mathbf{q},t)$ has been simulated by Lai and Fuller[30] for simple shear flow, who found that the structure factor elongates perpendicular to the direction of flow (i.e., the fluctuations in real space elongate in the direction of fluid flow). However, the above expression includes contributions from all spatial gradients in the velocity field. We can, therefore, capture the time evolution of $S(\mathbf{q},t)$ in a system where the velocity fields not only vary with time, but are also nontrivial.

For computational reasons, it is desirable to rewrite the above expression in dimensionless units and also to consider variations in the structure factor rather than the structure factor directly. In converting the above expressions into dimensionless units we follow the approach of Lai and Fuller. The dimensionless scattering factor is given by $\mathbf{k} \equiv \xi\mathbf{q}$, where ξ is the quiescent correlation length of the fluctuations. The correlation length is given by $\xi \equiv \sqrt{Mt_L}$, which simply relates the length and time scales. The dimensionless time is given by $\tau \equiv t/t_L$ where t_L is the stress relaxation time. The interfacial thickness is defined as $\epsilon \equiv \sqrt{\kappa/(2\chi_s - 2\chi)}$, and $L \equiv \epsilon^2/\xi^2$ is the square of the ratio between the interfacial width and the correlation length.

We have found it computationally more efficient to evolve the variations in structure factor, from the quiescent structure factor, rather than evolve the structure factor directly. The variation in structure factor, $\Delta S_{\mathbf{k}}$, is defined by

$$S_{\mathbf{k}} = S_{\mathbf{k}0} + \Delta S_{\mathbf{k}} = \frac{1}{(2\chi_s - 2\chi)(1 + Lk^2)} + \Delta S_{\mathbf{k}} \quad (10)$$

where $S_{\mathbf{k}0}$ is the equilibrium structure factor in the absence of imposed velocity fields. Making these substitutions we obtain the following evolution equation

$$\frac{\partial \Delta S_{\mathbf{k}}}{\partial \tau} = k_x \left[\frac{\partial v_x}{\partial x}\frac{\partial S_{\mathbf{k}0}}{\partial k_x} + \frac{\partial v_x}{\partial y}\frac{\partial S_{\mathbf{k}0}}{\partial k_y} + \frac{\partial v_x}{\partial z}\frac{\partial S_{\mathbf{k}0}}{\partial k_z} \right] + k_y \left[\frac{\partial v_y}{\partial x}\frac{\partial S_{\mathbf{k}0}}{\partial k_x} + \frac{\partial v_y}{\partial y}\frac{\partial S_{\mathbf{k}0}}{\partial k_y} + \frac{\partial v_y}{\partial z}\frac{\partial S_{\mathbf{k}0}}{\partial k_z} \right] + k_z \left[\frac{\partial v_z}{\partial x}\frac{\partial S_{\mathbf{k}0}}{\partial k_x} + \frac{\partial v_z}{\partial y}\frac{\partial S_{\mathbf{k}0}}{\partial k_y} + \frac{\partial v_z}{\partial z}\frac{\partial S_{\mathbf{k}0}}{\partial k_z} \right] + k_x \left[\frac{\partial v_x}{\partial x}\frac{\partial \Delta S_{\mathbf{k}}}{\partial k_x} + \frac{\partial v_x}{\partial y}\frac{\partial \Delta S_{\mathbf{k}}}{\partial k_y} + \frac{\partial v_x}{\partial z}\frac{\partial \Delta S_{\mathbf{k}}}{\partial k_z} \right] + k_y \left[\frac{\partial v_y}{\partial x}\frac{\partial \Delta S_{\mathbf{k}}}{\partial k_x} + \frac{\partial v_y}{\partial y}\frac{\partial \Delta S_{\mathbf{k}}}{\partial k_y} + \frac{\partial v_y}{\partial z}\frac{\partial \Delta S_{\mathbf{k}}}{\partial k_z} \right] + k_z \left[\frac{\partial v_z}{\partial x}\frac{\partial \Delta S_{\mathbf{k}}}{\partial k_x} + \frac{\partial v_z}{\partial y}\frac{\partial \Delta S_{\mathbf{k}}}{\partial k_y} + \frac{\partial v_z}{\partial z}\frac{\partial \Delta S_{\mathbf{k}}}{\partial k_z} \right] - 4(\chi_s - \chi)\mathbf{k}^2(1 + L\mathbf{k}^2)\Delta S_{\mathbf{k}} \quad (11)$$

where the derivatives of the velocity field are nondimensionalised with respect to the relaxation time and may be considered to vary as a function of time during the simulation. We can, therefore, simulate the evolution of the structure factor for a given element of fluid subject to complex time-dependent velocity fields.

We now consider the structure factor of the polymer blend along streamlines through the entire system, evolving the structure factor subject to the local velocity gradients. We simulate the evolution of the structure factor using eq 11. As already stated the quiescent interaction parameter is 9.5×10^{-4} and the correlation length is 6.4 nm. Given the degrees of polymerization, $N_A = 538$ and $N_B = 490$, the value of χ on the quiescent spinodal is 4.7×10^{-3}. The relaxation time, t_L, is of the order 1×10^{-3} s and the square of the ratio between correlation length and interfacial width is $L = 0.5$. We take the derivatives of the velocity field from our hydrodynamic simulations and initially evolve the simulation to equilibrium (total variation in $\Delta S_{\mathbf{k}} < 1 \times 10^{-10}$) given the velocity fields at $x = 0$ from the LB simulation. We then follow the streamline in the LB simulation from this point and evolve the structure factor subject to the local velocity gradients from the LB simulation. That is, we evolve the structure factor for an element of fluid as it *moves* through the slot die, varying the velocity gradients as a function of time.

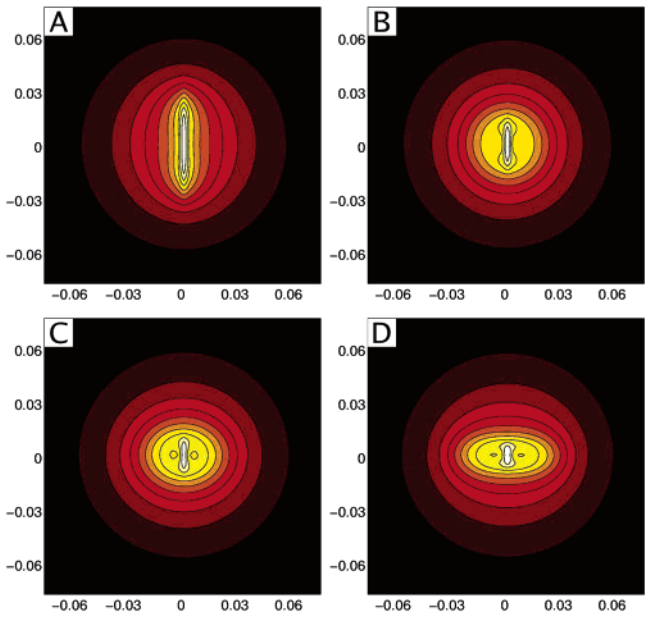

Figure 8. Structure factor in the q_x−q_y plane at various distances along the center streamline; q values are in units of Å^{-1}. The distances in the x-direction are (a) 0 (entrance), (b) 10, (c) 20 (exit), and (d) 21 mm.

Figure 8 shows the evolution of the structure factor (in the q_x−q_y plane) for a fluid element travelling through the center of the system (i.e., subject to the velocity derivatives shown in the upper graph of Figure 7. At the inlet of the slot die (Figure 8a) the structure factor is highly elongated in the q_y direction. The positive values of $\partial v_x/\partial x$, and negative values of $\partial v_y/\partial y$, "stretch" the fluid in the x-direction and "compress" the fluid in the y-direction. The result of which is that the fluctuations become highly oriented in the x-direction. As the fluid element moves through the center of the slot die the structure factor begins to relax back toward the quiescent state as the velocity gradients are negligible in this region. However, before the system can relax to an isotropic structure factor the fluid element reaches the outlet of the slot die. The positive values of $\partial v_y/\partial y$, and negative values of $\partial v_x/\partial x$, now elongate the domains of concentration fluctuations in the y direction, *perpendicular to the flow direction*. While this increases the domain size in the y direction, the system retains some memory of the orientation imposed on it at the inlet of the slot die. The result of this is that the structure factor exhibits orientation in the $q_y$direction for low wavevectors and elongation in the $q_x$direction for high wavevectors. In effect, because it takes longer to reorient fluctuations of larger size, the low wavevector regions of the structure factor remain elongated in the q_y direction, while at

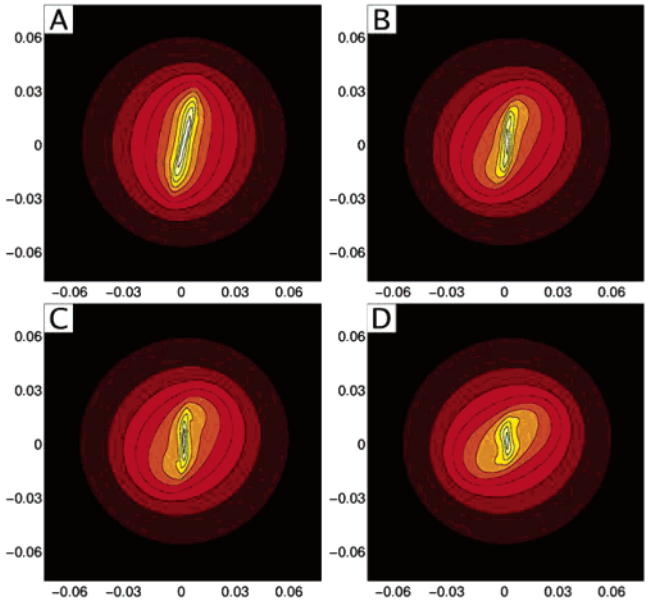

Figure 9. Structure factor in the q_x-q_y plane at various distances along an off-center streamline; q values are in units of Å^{-1}. The distances in the x-direction are (a) 0 (slot entrance), (b) 10, (c) 20 (exit), and (d) 21 mm.

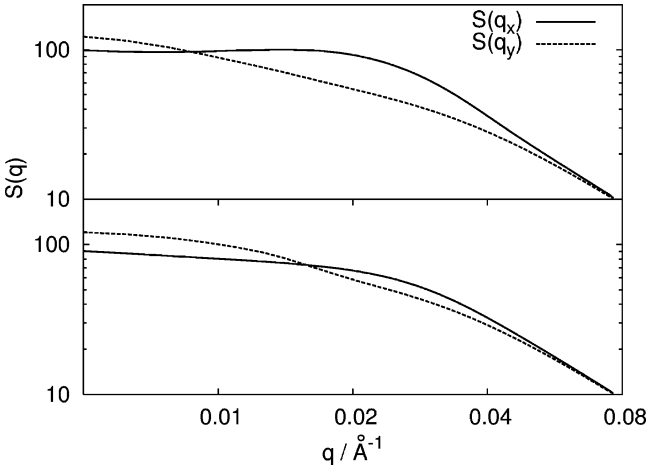

Figure 10. Structure factor in the q_x and q_y directions along the center (upper) and off-center (lower) streamlines at a position of 21 mm, 1 mm from the slot die exit.

high wavevectors the structure factor becomes elongated in the q_x direction much faster.

A similar effect is also seen in Figure 9, which follows a fluid element through the system away from the central streamline. That is, the fluid element starts 5 mm from the center in the y-direction and moves to within 0.5 mm of the center as the fluid element is contracted in the slot die. The velocity derivatives for this sreamline are given in the lower graph of Figure 7. In addition to the elongation of the fluctuations that was seen in the previous case due to velocity gradients $\partial v_x/\partial x$ and $\partial v_y/\partial y$, we now have the effects of velocity gradients $\partial v_x/\partial y$ and $\partial v_y/\partial x$. These velocity gradients represent pure shear and can result in the elongation and rotation of the fluctuations. This is evident in Figure 9 as the structure factor becomes elongated at an angle.

To gain further insights into these results we show one-dimensional profiles of the structure factor as a function of q_x and q_y in Figure 10. Figure 10a shows the profiles from the streamline through the center of the simulation, while Figure 10b shows the profiles from the off-center streamline. Both

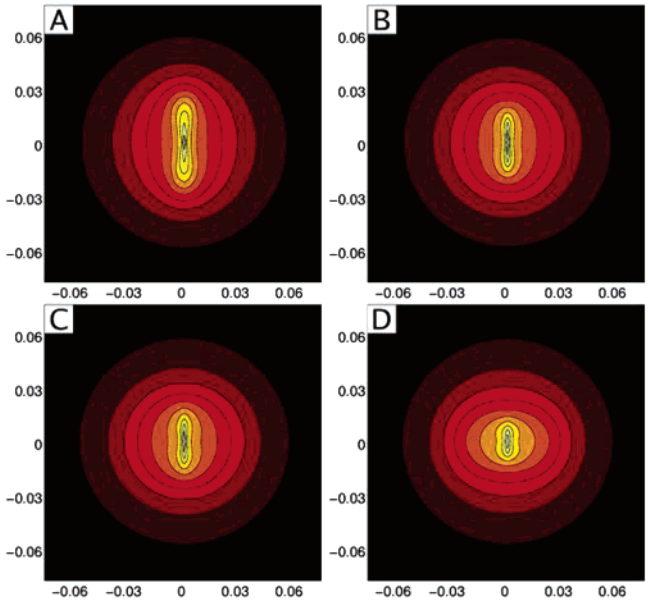

Figure 11. Structure factor in the q_x-q_y plane averaged over 15 different streamlines (see text); q values are in units of Å^{-1}. The distances in the x-direction are (a) 0 (inlet), (b) 10, (c) 20 (exit), and (d) 21 mm.

scattering patterns are depicted just outside the outlet of the slot die (at a position 1 mm from the outlet). These profiles highlight the elongation of the structure factor in q_y for low wavevectors, while the structure factor becomes elongated in q_x for higher wavevectors. The switch in the fluctuation orientation for the streamline travelling through the center occurs at ∼0.01 Å^{-1}, or at a fluctuation size of ∼10 nm. The off-center streamline sees a switch in fluctuation orientation at ∼0.015 Å^{-1}, or at a smaller fluctuation size of 6.6 nm. This is not surprising as the shear flow that the off-center streamline experienced would not only rotate the angle of fluctuation orientation but would also elongate the fluctuations in the flow direction. Therefore, the fluctuations become more elongated in the flow direction prior to leaving the slot die and elongation of the fluctuations perpendicular to the flow direction at the slot die exit are suppressed. The effects of this are to elongate only smaller fluctuations perpendicular to the flow direction at the outlet and to a lesser degree.

Experimentally, it is not possible to follow streamlines through the fluid as we have done numerically and the experimental results are averaged over a given area of the cell (in the $x-y$ plane) and through the entire thickness of the cell in the z-direction. Therefore, to gain a better understanding of the comparison between our numerical and experimental studies we average our simulation results over several streamlines at a given distance in the x-direction. In particular, we take sreamlines starting in the center of the channel and at ±2.5 and ±5 mm in the y-direction and at ±0.6 mm in the z-direction (making a total of 15 streamlines). Therefore, we consider streamlines not only in the central $x-y$ plane but also in off-central $x-y$ planes where the fluid experiences considerable velocity gradients in the z-direction. The average structure factors from these streamlines for varying positions in the x direction are depicted in Figure 11.

The cell is symmetric about the flow center line, and the streamlines considered reflect this symmetry, therefore the averaged structure factors are also symmetric. As the fluid passes through the inlet of the slot die the averaged structure factor is elongated, to it greatest degree, in q_y (spatial domain orientated

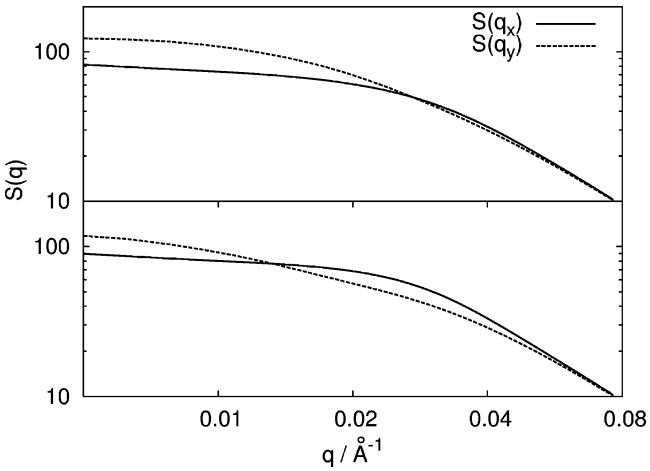

Figure 12. Structure factor in the q_x and q_y directions at positions of 20 (upper) and 21 mm (lower) in the *x*-direction. Profiles are averaged over 15 different streamlines (see text).

in the flow direction). This elongation subsides slightly as the fluid flows through the slot die. As the fluid emerges from the slot die, the fluctuations become elongated in the *y* direction for a short period of time. This is reflected by the elongation of the structure factor in q_x for large wavevectors. To quantify this effect, and the transition from fluctuation elongation in the *x* to the *y* direction, we show the one-dimensional profiles of $S(q)$ at the exit of the slot die (at 20 and 21 mm from the entrance) in Figure 12. The upper plot shows the structure factor at 20 mm, and the lower plot at 21 mm, both of which are sampled by the beam at position 4. At a position of 20 mm, at the exit of the slot die, the fluctuations appear to be elongated in the flow direction for larger fluctuations, and essentially isotropic for smaller fluctuations. This is seen by $S(q_x)$ being lower than $S(q_y)$ at low wavevectors while for higher wavevectors there is little difference between $S(q_x)$ and $S(q_y)$. For the averaged structure factor at 21 mm, just outside the slot die, the larger fluctuations remain oriented in the flow direction, but now the smaller fluctuations appear to be oriented *perpendicular* to the flow direction. In the averaged structure factor calculated here, it is worth noting that this effect is likely to be suppressed by the velocity gradients in the *z*-direction, which tend to orient concentration fluctuations in the flow direction.

By comparison between our experimental and simulations results, it is clear that by including only convective effects, we do not achieve even qualitative agreement with the observed behavior. In particular, our experimental results show the concentration fluctuations to be elongated perpendicular to the flow direction, while our simulations, which assume simple convective effects, predict the concentration fluctuations to be elongated in the flow direction.

Stress Gradients. Since, in polymeric systems, the viscosity depends sensitively on the molecular weight as well as on the chemical structure, in a mixture in which concentration fluctuations are present there will be resultant stress gradients. The principal works in which the effects of the latter on the dynamics of such fluctuations in polymer solutions have been considered are by Helfand and Fredrickson,[38] Onuki,[39] and Milner.[40] Doi and Onuki[41] extended the models to polymer blends in which both components are entangled. The key aspect to address is how to incorporate stress into the equation of motion for concentration fluctuations. Effectively, by determining the conditions for force balance, it was shown that the stress enters the equation of motion at the same level as the chemical potential. Such an approach enabled the development of a framework that coupled the dynamics of concentration fluctuations to the flow fields and stress gradients; however, only the simplest form of constitutive relation for the stress was treated. Doi and Onuki[41] assumed that the dynamics of stress relaxation were well described by a single relaxation time.

A significant feature of the rheological behavior of polymer blends is that, in general, stress relaxation cannot be adequately described using a single relaxation time. Clarke and McLeish,[42] Clarke,[43] Sun et al.[44] and Criado-Sancho et al.[45] have attempted to address this shortcoming. Sun et al.[44] proposed a model in which the shear modulus of the blend was allowed to be concentration dependent, while other authors[42,43,45] introduced a specific mixing rule, which also included finite relaxation times for each of the components. In all models, stress was incorporated into the modified Cahn−Hilliard equation of motion for concentration fluctuations derived by Doi and Onuki.[41] However, extending the model to incorporate a generalized flow field of the form represented by eq 8 is nontrivial and has yet to be attempted. Hence, here we summarize the consequences of a simple shear flow on the structure factor when stress gradients are taken into account.

To understand the essential physical phenomena that occur when blends are sheared, Doi and Onuki utilized Rayleigh's variational principle, which amounts to minimizing the energy dissipation function with respect to the average velocities of the two components. The resultant equation of motion for the structure factor is

$$\frac{\partial S(\mathbf{q},t)}{\partial t} - \dot{\gamma} q_x \frac{\partial S(\mathbf{q},t)}{\partial q_y} = -2M\left[2q^2(\chi_S - \chi + \kappa q^2) - \frac{\alpha}{k_B T}\sum_{i,j} q_i q_j \frac{\partial}{\partial \phi_A}\sigma_{ij}^{(n)}\right] S(\mathbf{q},t) + 2Mq^2 \quad (12)$$

The σ_{ij} represent the various components of the stress tensor, all of which can be expected to depend on composition, and α is a parameter dependent on the number of entanglements per chain and the monomeric friction coefficients.[41] Without stress gradients, i.e., for a blend whose components have identical responses to shear, eq 12 reduces to eq 6, as would be expected. Again, for the simple shear flow under consideration in this section, q_x, q_y, and q_z are the wavevectors in the flow, flow-gradient, and vorticity directions, respectively.

To gain some analytical insight, it is useful to focus our attention on the q_y and q_z directions. In these directions, the convective term of eq 12 vanishes, and an effective diffusion coefficient, D_{eff} may be defined using,

$$\frac{\partial S(q_{y,z},t)}{\partial t} = -2q_{y,z}{}^2 D_{\text{eff}}(q_{y,z}) S(q_{y,z},t) + 2Mq_{y,z}{}^2 \quad (13)$$

which is no more than the Cahn−Hilliard equation for the dynamics of concentration fluctuations with a modified diffusion coefficient which depends on gradients in the stress as well as gradients in the chemical potential. In particular, the stress components of relevance[43] are the normal stresses, σ_{xx} and σ_{yy}, since shear stresses do not act along the q_y and q_z directions. From eqs 12 and 13, the effective diffusion coefficients in the q_y and q_z directions are given by

$$D_{\text{eff}}(q_i) = 2M(\chi_s - \chi + \kappa q_i{}^2) - \frac{M}{k_B T}\frac{\partial \sigma_{ii}}{\partial \phi_A} \equiv 2M[\chi_s - \chi + \kappa q_i{}^2 + \Delta\chi_s(q_i)](i = y, z) \quad (14)$$

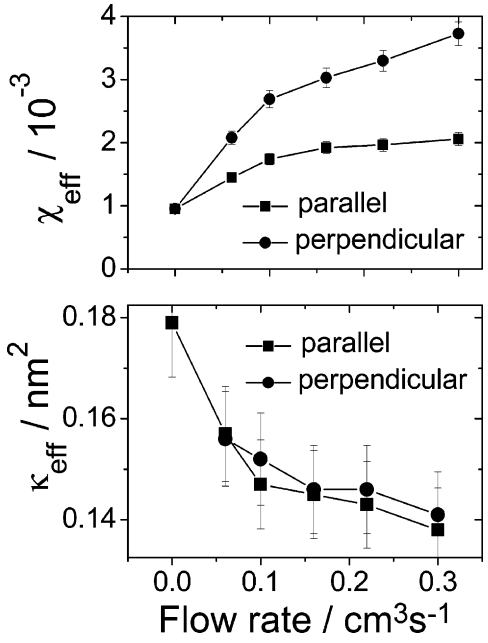

Figure 13. (a) Effective interaction parameter and (b) effective interfacial energy parameter as a function of flow rate at position 2. The increase in the interaction parameter with flow rates is a consequence of flow induced enhancement of fluctuations.

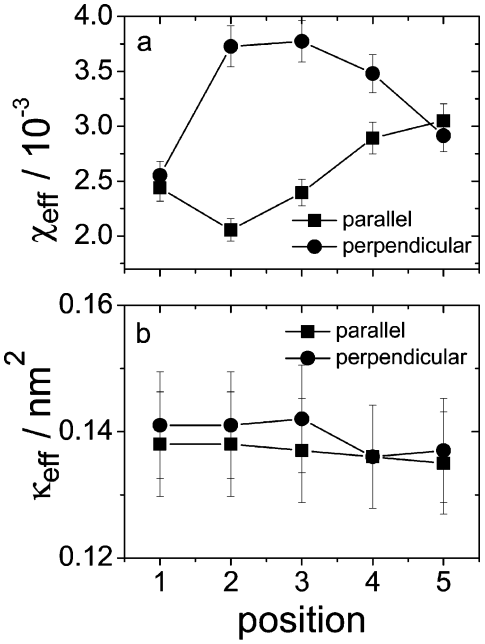

Figure 14. (a) Effective interaction parameter and (b) effective interfacial energy parameter as a function of position, at the maximum flow rate.

which serves to define $\Delta\chi_s(q_y)$ and $\Delta\chi_s(q_z)$. Importantly, both depend on the variation of the normal stresses with concentration. Without such a variation, $\Delta\chi_s(q_y) = \Delta\chi_s(q_z) = 0$ and as a consequence the structure factor in the q_y and q_z directions would be unperturbed by the flow. Example expressions, in the limit of $q \rightarrow 0$, in terms of relaxation times and plateau modulae, for a specific blend constitutive equation can be found elsewhere.[43] If $\Delta\chi_s > 0$, fluctuations are suppressed, whereas if $\Delta\chi_s < 0$, fluctuations are enhanced. In the latter case, the magnitude of $\Delta\chi_s$ may be sufficient for D_{eff} to become negative so that fluctuations become unstable and grow. Combining eqs 13 and 14, we find that in the steady state,

$$S(q_i) = \frac{1}{2[\chi_s - \chi + \kappa q_i^2 + \Delta\chi_s(q_i)]} \tag{15}$$

This result presents a physical explanation for why an Ornstein−Zernike type expression should be valid in the presence of a flow field. Although the theory is not strictly valid in the flow direction, we now consider that eq 15 provides a reference with which to understand our observation that the scattering is well described by the general form given by eq 3 in the steady state, such that

$$S(q_i) = \frac{1}{2[\chi_s - \chi_{eff} + \kappa_{eff} q_i^2]} \tag{16}$$

where χ_{eff} and κ_{eff} are related to S_0 and the correlation length by direct comparison with eq 3. The resultant values for the effective interaction parameter and the effective interfacial energy parameter are shown in Figure 13 for position 2, and for all positions for the maximum flow rate in Figure 14. While the effective interaction parameter is seen to increase significantly with flow rate (a factor of 4 increase at the highest flow rate relative to the quiescent value), the decrease in the effective interfacial energy is much less significant, suggesting that the latter is mostly unperturbed by the flow. These results further support our assertion that chain stretching is negligible: Pistoor and Binder[46] showed that a model that incorporates affine chain stretching in addition to convection, but does not include stress gradients, results in a modification of the effective interfacial energy but not the interaction parameter.

4. Conclusions

We have found that fluctuations in polymer blends subjected to a contraction−expansion flow become enhanced with increasing flow rate. The data can be interpreted in terms of an effective interaction parameter, which reflects the coupling between flow and thermodynamics. As noted in the Introduction, previous experiments using a concentric cylinder shear cell observed the suppression of fluctuations for two very different blends by shear. This is in stark contrast to the observation that we have reported. The difference mirrors the complexity of observations for the effects of flow on miscibility.

In view of the failure of the numerical investigation to even qualitatively capture the experimental observations, we believe that the existence of normal forces is key to explaining our experimental observations. Since the degrees of polymerization of the two components are similar, it is worth considering what gives rise to viscous stress imbalances. Most probably they arise from the large difference in glass transition temperature between the two components. Poly(α-methylstyrene) has a glass transition temperature[25] of ∼170 °C, which is ∼70 °C higher than that of polystyrene, so at any given temperature, if the two components have similar molecular weights, it might be expected that PαMS will have a higher viscosity. Hence any regions that are slightly richer in PαMS will also have a greater viscosity than regions slightly richer in PS. Therefore, even small fluctuations in concentration could give rise to considerable gradients in the weakly non-Newtonian stresses.

Unlike block copolymers, surfactant systems and even demixed polymers, there have been relatively few studies on partially miscible polymer blends in a flow, and in particular on the coupling between flow and concentration fluctuations in the one-phase region. This would appear, in part, to be related to the difficulty in developing equipment that is able to produce the high torque necessary to shear high molecular weight

polymer mixtures. Only through systematic and wide ranging studies will it be possible to quantitatively test some of theoretical ideas currently being developed. Recently there has been an increase in studies on the dynamics of miscible polymer blends, with predictions of the composition dependence of blend rheology becoming increasingly quantitative.[47] Such blends offer a promising avenue for testing theories that couple thermodynamics with flow, since the rheological response can be unambiguously determined without concerns that arise when phase boundaries are approached.[48] We emphasize that a theoretical framework that aims to predict stability limits must be able to also predict scattering patterns. We hope that the experimental, computational and theoretical results presented in this paper will stimulate further studies of polymer blends subjected to flows.

References and Notes

(1) Mazich, K. A.; Carr, S. H. *J. Appl. Phys.* **1983**, *54*, 5511.
(2) Hindawi, I. A.; Higgins, J. S.; Weiss, R. A. *Polymer* **1992**, *33*, 2522.
(3) Fernandez, M. L.; Higgins, J. S.; Horst, R.; Wolf, B. A. *Polymer* **1995**, *36*, 149.
(4) Hong, Z.; Shaw, M. T.; Weiss, R. A. *Polymer* **2000**, *41*, 5895.
(5) Katsaros, J. D.; Malone, M. F.; Winter, H. H. *Polym. Bull. (Berlin)* **1986**, *16*, 83.
(6) Katsaros, J. D.; Malone, M. F.; Winter, H. H. *Polym. Eng. Sci.* **1989**, *29*, 1434.
(7) Larbi, F. B. C.; Malone, M. F.; Winter, H. H.; Halary, J. L.; Leviet, M. H.; Monnerie, L. *Macromolecules* **1988**, *21*, 3532.
(8) Madbouly, S. A.; Ougizawa, T.; Inoue, T. *Macromolecules* **1999**, *32*, 5631.
(9) Mani, S.; Malone, M. F.; Winter, H. H. *Macromolecules* **1992**, *25*, 5671.
(10) Mani, S.; Malone, M. F.; Winter, H. H.; Halary, J. L.; Monnerie, L. *Macromolecules* **1991**, *24*, 5451.
(11) Clarke, N. In *Phase Behavior of Polymer Blends*; Freed, K. F., Ed.; Springer-Verlag: Berlin, 2005; Vol. 183, p 127.
(12) Horst, R.; Wolf, B. A. *Macromolecules* **1993**, *26*, 5676.
(13) Clarke, N.; McLeish, T. C. B. *Macromolecules* **1999**, *32*, 4447.
(14) Gerard, H.; Higgins, J. S.; Clarke, N. *Macromolecules* **1999**, *32*, 5411.
(15) Cahn, J.; Hilliard, J. *J. Chem. Phys.* **1958**, *28*, 258.
(16) deGennes, P. *Scaling Concepts in Polymer Physics*; Cornell University Press: Ithaca, NY, 1980.
(17) Flory, P. J. *Principles of Polymer Chemistry*; Cornell University Press: Ithaca, NY, 1953.
(18) Nakatani, A. I.; Kim, H. D.; Takahashi, Y.; Matsushita, Y.; Takano, A.; Bauer, B. J.; Han, C. C. *J. Chem. Phys.* **1990**, *93*, 795.
(19) Saito, S.; Hashimoto, T.; Morfin, I.; Lindner, P.; Boue, F.; Pine, D. J. *Macromolecules* **2003**, *36*, 3745.
(20) Saito, S.; Koizumi, S.; Matsuzaka, K.; Suehiro, S.; Hashimoto, T. *Macromolecules* **2000**, *33*, 2153.
(21) Miroshnychenko, D.; Clarke, N. *Phys. Rev. E* **2002**, *66*, 041802.
(22) Clarke, N.; Miroshnychenko, D. *Phys. Rev. E* **2005**, *71*, 031804.
(23) Rothstein, J. P.; McKinley, G. H. *J. Non-Newtonian Fluid Mech.* **2001**, *98*, 33.
(24) Kim, J. K.; Han, C. D. *Macromolecules* **1992**, *25*, 271.
(25) Lin, J. L.; Roe, R. J. *Macromolecules* **1987**, *20*, 2168.
(26) Bent, J.; Hutchings, L. R.; Richards, R. W.; Gough, T.; Spares, R.; Coates, P. D.; Grillo, I.; Harlen, O. G.; Read, D. J.; Graham, R. S.; Likhtman, A. E.; Groves, D. J.; Nicholson, T. M.; McLeish, T. C. B. *Science* **2003**, *301*, 1691.
(27) Bent, J. F.; Richards, R. W.; Gough, T. D. *Rev. Sci. Instrum.* **2003**, *74*, 4052.
(28) We note that the experiments reported in this paper were undertaken during the first 12 h of a 48 h allocation of beamtime. The blend was subjected to a number of further flow experiments at a range of temperatures. Hence the 4% degradation should be considered as a maximum value.
(29) Cook, H. E. *Acta Metall. Acta Metall.* **1970**, *18*, 297.
(30) Lai, J.; Fuller, G. G. *J. Polym. Sci., Part B: Polym. Phys.* **1994**, *32*, 2461.
(31) Ohta, T.; Nozaki, H.; Doi, M. *J. Chem. Phys.* **1990**, *93*, 2664.
(32) Chen, S.; Doolen, G. D. *Annu. Rev. Fluid Mech.* **1998**, *30*, 329.
(33) d'Humieres, D.; Ginzburg, I.; Krafczyk, M.; Lallemand, P.; Luo, L. S. *Philos. Trans. R. Soc. London Ser. A—Math. Phys. Eng. Sci.* **2002**, *360*, 437.
(34) Frisch, U.; d'Humieres, D.; Hasslacher, B.; Lallemand, P.; Pomeau, Y.; Rivet, J.-P. *Comple Syst.* **1987**, *1*, 649.
(35) Ladd, A. J. C.; Verberg, R. *J. Stat. Phys.* **2001**, *104*, 1191.
(36) Canceliere, A.; Chang, C.; Foti, E.; Rothman, D. H.; Succi, S. *Phys. Fluids a: Fluid Dyn.* **1990**, *2*, 2085.
(37) Buxton, G. A.; Verberg, R.; Jasnow, D.; Balazs, A. C. *Phys. Rev. E* **2005**, *71*, 056707.
(38) Helfand, E.; Fredrickson, G. H. *Phys. Rev. Lett.* **1989**, *62*, 2468.
(39) Onuki, A. *J. Phys. Soc. Jpn.* **1990**, *59*, 3427.
(40) Milner, S. T. *Phys. Rev. Lett.* **1991**, *66*, 1477.
(41) Doi, M.; Onuki, A. *J. Phys. II* **1992**, *2*, 1631.
(42) Clarke, N.; McLeish, T. C. B. *Phys. Rev. E* **1998**, *57*, R3731.
(43) Clarke, N. *Faraday Discuss.* **1999**, *112*, 249.
(44) Sun, T.; Balazs, A. C.; Jasnow, D. *Phys. Rev. E* **1999**, *59*, 603.
(45) Criado-Sancho, M.; Jou, D.; Casas-Vazquez, J.; del Castillo, L. F. *Phys. Rev. E* **2002**, *66*, 061803.
(46) Pistoor, N.; Binder, K. *Colloid Polym. Sci.* **1989**, *266*, 132.
(47) Pathak, J. A.; Kumar, S. K.; Colby, R. H. *Macromolecules* **2004**, *37*, 6994.
(48) Sharma, J.; Clarke, N. *J. Phys. Chem. B* **2004**, *108*, 13220.

MA0610966